Diffraction of strong shocks by cones, cylinders, and spheres

By A. E. BRYSON
Harvard University
AND R. W. F. GROSS*
Douglas Aircraft Company, Inc.

(Received 24 July 1960)

This paper presents experimental investigations of the diffraction of plane strong shocks by several cones, a cylinder, and a sphere. The diffraction pattern, in particular the loci of Mach triple points and the shape of the diffracted shocks are compared with theoretical results obtained from a diffraction theory proposed by Whitham (1957, 1958, 1959). The agreement between theory and experiment is shown to be good. Also given are extensive numerical results supplementing Whitham's papers, and theoretical considerations applying Whitham's theory to very blunt bodies.

1. Introduction

Whitham (1957, 1958, 1959) has presented an approximate theory for the dynamics of two- and three-dimensional shock waves. He applied this theory to the description of shock diffractions on wedges and a cone of 28·8° semi-angle. The present paper presents experimental results of shock diffractions by several cones with different apex angles at shock Mach numbers between 3·5 and 4·0 and compares them with numerical solutions obtained using Whitham's theory. In addition, Whitham's theory is extended to blunt two- and three-dimensional bodies, in particular a cylinder and a sphere. A theory based on Whitham's ideas is presented to describe the diffraction pattern near the nose of very blunt bodies. This theory was used to find initial values, at a distance sufficiently far from the nose to start a characteristics solution of Whitham's equations for the sphere and the cylinder. The agreement between theory and experiment at shock Mach numbers near 3·00 for certain features of the diffraction pattern was found to be good.

2. Experimental investigations and their results

The experimental investigations were performed in the Harvard University 4 in. × 12 in. × 40 ft. shock tube in air. A Schlieren optical system using a spark light source of approximately 0·2 μsec duration was used to photograph the

* Formerly Harvard University.

diffraction patterns. The shock speed was measured between two Schlieren light screens by means of an electronic counter. The second light screen also triggered a variable time delay which in turn triggered the spark light source.

Diffraction on cones

A series of Schlieren pictures of diffractions on cones with semi-apex angles θ_w varying between 9·7° and 44·7° was taken at a mean shock Mach number of $3{\cdot}68 \pm 0{\cdot}16$. Figure 1 (plate 1) gives a typical photograph from this series.

The feature of the diffraction pattern predicted by Whitham's theory is the shape and location of the diffracted shock (Mach shock) at any time. The theory

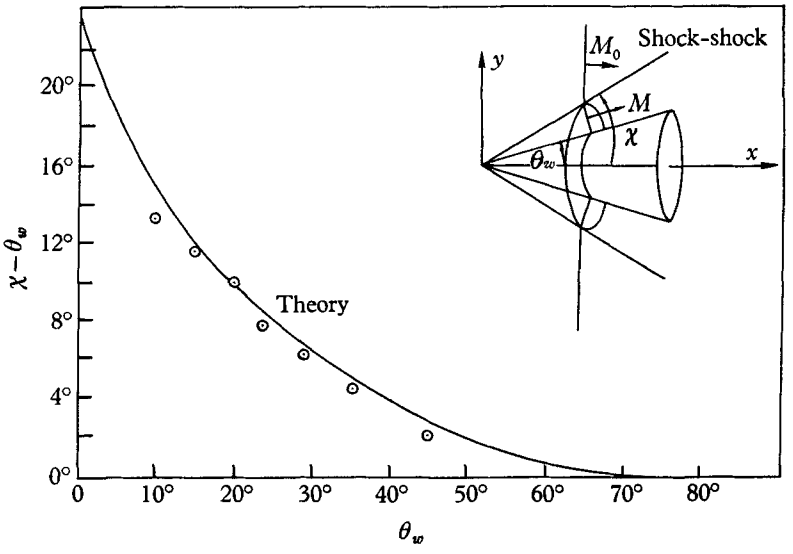

FIGURE 2. Shock-shock angle χ *vs* cone semi-apex angle θ_w for shock Mach number $M_0 = 3{\cdot}68$. ⊙ Exp. points.

does not predict the shape or location of reflected shocks. As part of the description of the Mach shock, the locus of successive positions of the Mach triple point can be found. Whitham calls this locus a 'shock-shock', since it represents a (Mach) shock moving along the incident shock.

Shock-shocks of any conical diffraction are straight lines inclined by an angle χ (shock-shock angle) with respect to the axis of symmetry. This angle was determined from the photographs. Figure 2 shows $\chi-\theta_w$ *vs* θ_w compared with the curve predicted by Whitham's theory for incident Mach number $M_0 = 3{\cdot}68$. As is seen the experimental points lie below the theoretical curve. This is the same discrepancy as that reported by Whitham (1957) on wedges. It appears to be connected with the fact that this theory does not allow for the possibility of a regular reflexion. Instead, this theory predicts Mach reflexion for all angles θ_w up to 90°, although $\chi-\theta_w$ becomes so small for $\theta_w > 70°$ that one could consider it a regular reflexion for all practical purposes.

Except for very small semi-apex angles θ_w the Mach shock is predicted to

be almost a straight line. This is shown to be true (figure 1, plate 1) although at very small θ_w the shock is so weak that an accurate determination from the Schlieren pictures was not possible.

Diffraction on a cylinder

The most extensive results were obtained for a cylinder of diameter $D = \frac{1}{2}$ in. Each shock-tube run produced one picture of the diffraction in a certain stage of development. Figures 3–5 (plates 2–4) show typical examples.

Two series of experiments were performed at the same mean shock Mach number of 2·82 but at two different pressures P_2 behind the undisturbed shock

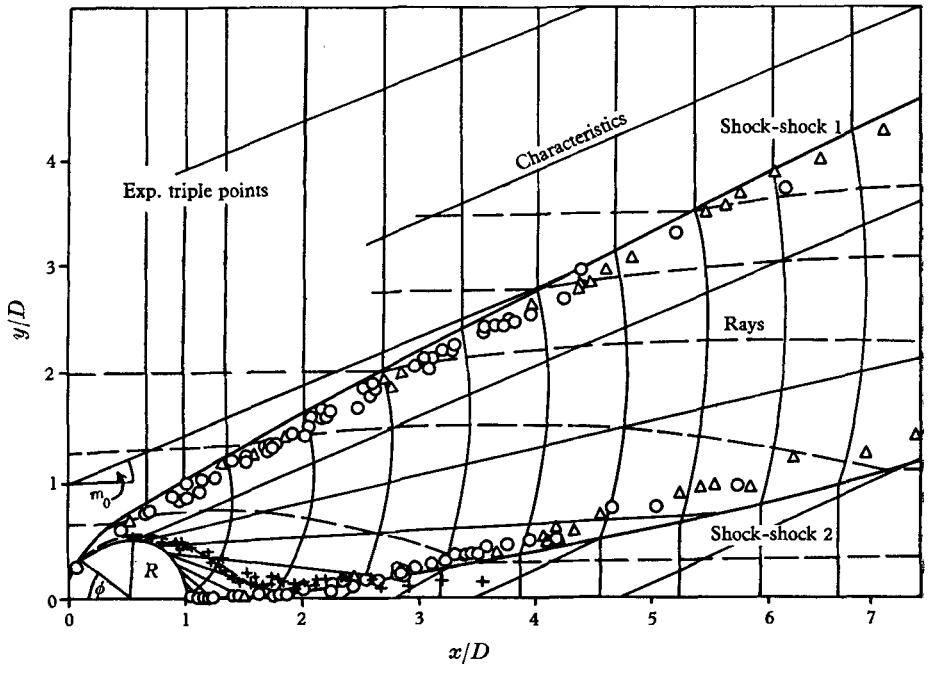

FIGURE 6. Diffraction on a cylinder. $M_0 = 2{\cdot}81$. ○ $Re = 7{\cdot}79 \times 104$, △ $Re = 0{\cdot}87 \times 10^4$, +vortex locus.

and, therefore, at two different Reynolds numbers, $Re = uD/\nu$ (u being the velocity of the undisturbed shock afterflow, D the diameter of the cylinder and ν the kinematic viscosity behind the undisturbed shock):

Series 1, $P_2 = 9{\cdot}94$ p.s.i., $Re = 7{\cdot}79 + 10^4$;

Series 2, $P_2 = 1{\cdot}08$ p.s.i., $Re = 0{\cdot}78 + 10^4$.

The diffraction was followed through about 7 diameters of travel of the incident shock past the cylinder.

On a cylinder two loci of triple points appear on either side of the plane of symmetry of the flow, one starting at the front of the cylinder, and the other at the plane of symmetry behind the cylinder (figures 4 and 5, plates 3 and 4). One half of the symmetrical diffraction pattern is shown in figure 6, which summarizes the data of the two series of experiments on the cylinder, together with the predicted shock-shocks using Whitham's theory.

When the incident shock first impinges on the cylinder a regular reflexion is formed since $\theta_w > \theta_{w\max}$, the cut-off angle. Between 40° and 50° from the forward stagnation point Mach reflexion begins. Figure 3 (plate 2), therefore, shows two curved Mach shocks and the corresponding slip surfaces just before the Mach shocks meet at the rear end of the cylinder. Note that the slip surface has 'rolled up' into a vortex (not to be mistaken for the vortices formed in viscous flow *behind* a cylinder). This vortex is formed in a boundary-layer shock-wave interaction at the time when the Mach shock is first created. The vortex was not observed in series 2 experiments; the low density and resulting decreased Schlieren sensitivity probably rendered it invisible. If the assumption is made that the circulation of the vortex does not change very much with time, it should follow a particle path. The locus of vortex positions is also shown in figure 6. Whitham, calling the orthogonal trajectories of the shock positions rays, assumes that they are identical with particle paths; note that the vortex follows a ray closely except as it nears the plane of symmetry of the flow behind the cylinder.

The interaction of the two Mach shocks as they collide behind the cylinder may be considered as a reflexion off a solid wall in place of the plane of symmetry. Here again the reflexion is at first regular, Mach reflexion beginning between 0·5 and 1·0 diameters behind the cylinder. This second Mach reflexion is evident in figures 4 and 5 (plates 3 and 4).

In figure 3 (plate 2) boundary-layer separation is seen to take place on the aft sides of the cylinder. Figures 4 and 5 (plates 3 and 4) show the flow field resulting from the interaction between reflected shocks and the separated boundary-layer material behind the cylinder during the process of wake formation. In spite of this complicated flow behind the diffracted shocks, agreement between the predicted diffraction pattern and experiments appears to be good. Note in particular that a change of Reynolds number by a factor of 10 did not result in any change of the loci of the triple points in the diffraction pattern.

Diffraction on a sphere

Two series of Schlieren photographs of the diffraction on a sphere were taken in the same manner as for the cylinder. An English table-tennis ball of 1 in. diameter filled with Wood's metal and suspended in the test section from 8 nylon strings was used for a sphere. Having found the Reynolds number of no influence on the diffraction pattern, it was kept (approximately) constant and the diffraction investigated at two incident shock Mach numbers $M_0 = 2{\cdot}85$ and $M_0 = 4{\cdot}41$. Due to the larger size of the sphere the experiments cover the diffraction over a range of only 3·5 sphere-diameters of travel of the incident shock. The diffraction pattern for a sphere is qualitatively the same as for the cylinder: two pairs of triple-point loci appear on either side of the axis of symmetry. Figures 7 and 8 (plates 5 and 6) show instances in the development of the diffraction (the radial lines are the nylon strings). The diffraction pattern behind the sphere shows a spherical shock penetrating the straight Mach shock (figure 8, plate 6). This spherical shock is the reflected shock resulting from the point collision of the converging cylindrical Mach shock at the rear stagnation point of the sphere.

Due to the small extension of the disturbed flow field normal to the direction of propagation, the viscous wake development as well as the slip surfaces are almost invisible to the Schlieren system.

Figure 9 shows the experimentally found loci of the triple points plotted together with the shock-shock obtained from the theory by the method of characteristics for incident Mach numbers $M_0 \gg 1$. Due to difficulties in extending the

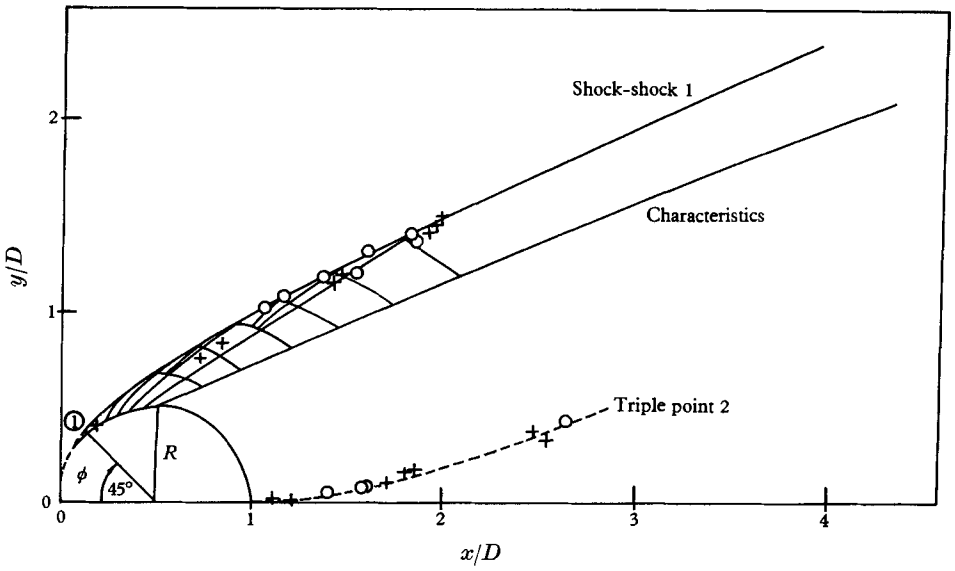

FIGURE 9. Diffraction on a sphere; characteristics solution for $M_0 \gg 1$. Exp. triple points: ○ $M_0 = 2{\cdot}85$, + $M_0 = 4{\cdot}41$, ① starting of characteristic solution.

characteristics net around the sphere to its back side, no theoretical prediction for the second shock-shock could be obtained. The agreement between theory and experiment along the first shock-shock is good. Whitham's theory predicts that the diffraction pattern should be the same for incident Mach numbers $M_0 \geqslant 3$. This is substantiated by the coincidence of the loci of the triple points found experimentally for the two incident shock Mach numbers ($M_0 = 2{\cdot}85$ and $M_0 = 4{\cdot}41$) and the shock-shock predicted for $M_0 \gg 1$.

3. Theoretical calculations

Theoretical calculations cover (1) the numerical solutions of the equations governing conical flows (with a number of by-products, which have been tabulated for future reference); (2) a semi-graphical solution by the method of characteristics for the cylinder; and (3) a purely graphical solution by characteristics for the sphere. An attempt was made in the latter two cases to simplify the calculations as much as possible by exploiting the peculiarities of the diffraction equations. In order to find an initial value curve from which to start the characteristics solution, an approximate solution for the nose region of the cylinder and the sphere was developed, based on the fundamental ideas of

Whitham's theory. The approximation was also extended to cones of large semi-apex angles.

Solution of the conical equations

The equations governing conical diffractions given by Whitham (1959, equations 52, 53, 54) for finite incident Mach number M_0 were solved on a high-speed digital computer by simultaneous integrations, starting from the shock-shock and calculating backwards to the cone surface. The method has been described by Whitham (1959). Figure 10 shows the hodograph shock-shock

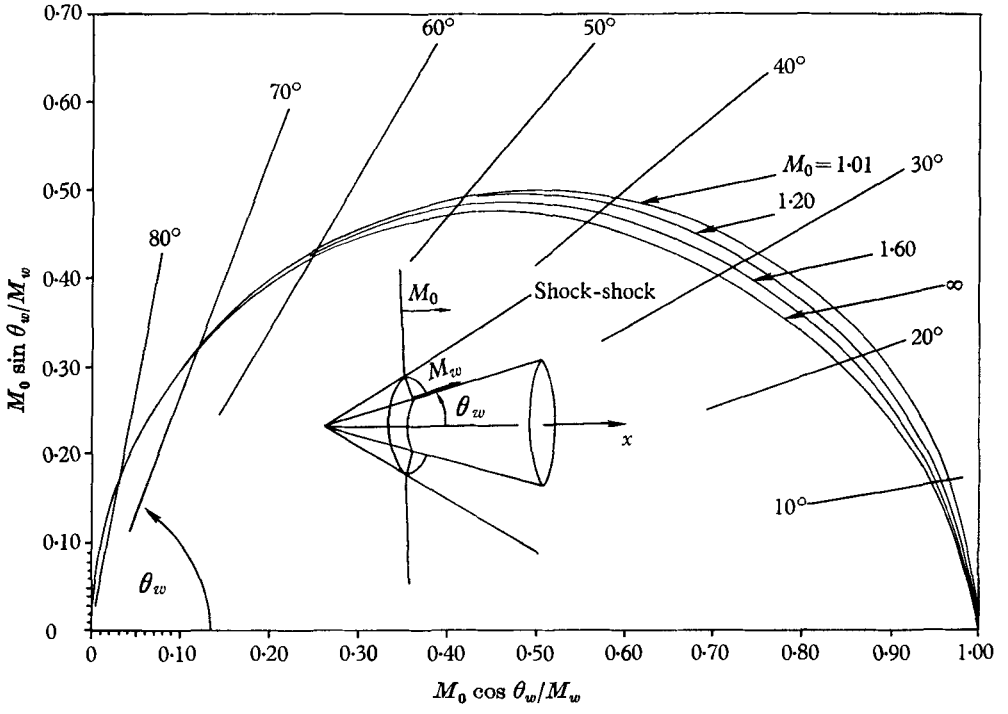

FIGURE 10. Crescent curves for conical diffractions.

polars which we will call 'crescent curves': M_0/M_w *vs* θ_w corresponding to one branch of Busemann's 'apple curves' in supersonic flow (M_0/M_w = relative Mach number on wall, θ_w = semi-apex angle) with M_0 as a parameter. Figure 11 gives $(\chi - \theta_w)$ *vs* θ_w with M_0 as a parameter. Also shown is the curve obtained from the approximate theory for cones of large semi-apex angles. Finally, figure 12 shows the full 'crescent curve' for $M_0 \gg 1$, including the curves representing the solutions of the conical diffraction in the hodograph plane. In order to make these calculations, it was necessary to determine, as functions of Mach number, the ray area A, the characteristic angle m, the integral function analogous to the Prandtl–Meyer function, ω, and the shock-shock jump conditions. Since these functions are not tabulated elsewhere, and appear to be of general interest for any further application of this theory, they are reproduced in table 1.

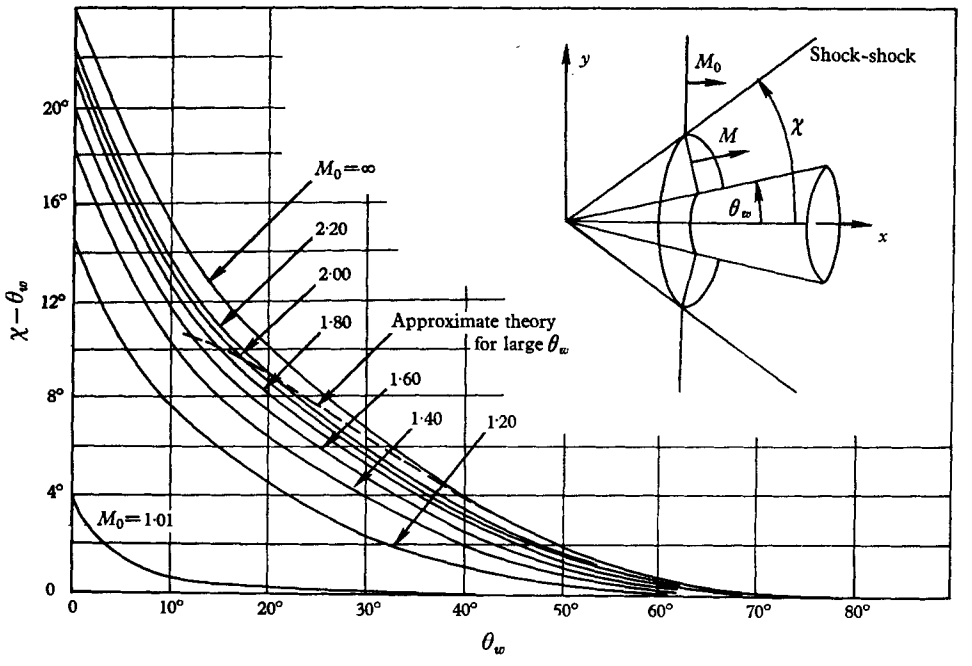

FIGURE 11. Shock-shock angle χ *vs* cone semi-apex angle θ_w.

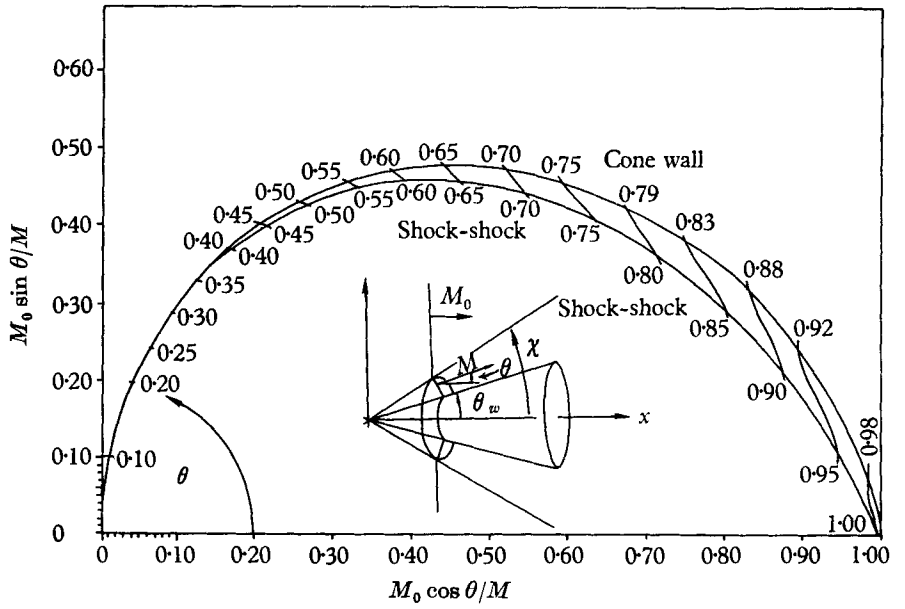

FIGURE 12. Complete crescent curves for conical diffractions. $M_0 \gg 1$.

The respective equations are given by Whitham (1957).

(1) Ray area, $A = A(M)$:

$$A = k\exp\left\{-\int \frac{2M\,dM}{(M^2-1)\,K(M)}\right\} = kf(M),$$

where
$$K(M) = 2\left[\left(1+\frac{2}{\gamma+1}\frac{1-\mu^2}{\mu}\right)\left(2\mu+1+\frac{1}{M^2}\right)\right]^{-1},$$

$$\mu^2 = \frac{(\gamma-1)M^2+2}{2\gamma M^2-(\gamma-1)},$$

and k is an arbitrary constant. As noted by Whitham this integral has an analytical solution which was found to be

$$\begin{aligned} f(M) = \exp\Bigg[\Bigg[&-\left\{\log\frac{M^2-1}{M}+\frac{1}{\gamma}\log\left(M^2-\frac{\gamma-1}{2\gamma}\right)+\log\frac{1-\mu}{1+\mu}\right. \\ &+\left(\frac{\gamma-1}{2\gamma}\right)^{\frac{1}{2}}\log\left[\mu+\left(\frac{2\gamma}{\gamma-1}\right)^{\frac{1}{2}}\right]-\left(\frac{\gamma-1}{2\gamma}\right)^{\frac{1}{2}}\log\left[\mu-\left(\frac{2\gamma}{\gamma-1}\right)^{\frac{1}{2}}\right] \\ &+\left(\frac{2}{\gamma(\gamma-1)}\right)^{\frac{1}{2}}\log\left[\left(M^2-\frac{2}{\gamma-1}\right)^{\frac{1}{2}}+\left(M^2-\frac{\gamma-1}{2\gamma}\right)^{\frac{1}{2}}\right] \\ &\left.+\left[\frac{1}{2(\gamma-1)}\right]^{\frac{1}{2}}\tan^{-1}\left\{\frac{[4\gamma-(\gamma-1)^2]M^2-4(\gamma-1)}{4\gamma^{\frac{1}{2}}(\gamma-1)(M^2+2/\gamma-1)^{\frac{1}{2}}(M^2-(\gamma-1)/2\gamma)^{\frac{1}{2}}}\right\}\right\}\Bigg]\Bigg] \end{aligned}$$

choosing $k = 1$. $A = f(M)$ is tabulated in table 1.

(2) The characteristic angle $m = m(M)$ is given by

$$m = \tan^{-1}\left[\frac{(M^2-1)\,K(M)}{2M^2}\right]^{\frac{1}{2}}.$$

Values for $m = m(M)$ are also tabulated in table 1.

(3) The integral ω corresponding to the Prandtl–Meyer function in supersonic flow is given by

$$\omega = \int_1^M \left[\frac{2}{(M^2-1)\,K(M)}\right]^{\frac{1}{2}} dM.$$

Therefore for two-dimensional diffractions the characteristics of Whitham's diffraction equations are given by

$$\theta \pm \omega = \text{const.}$$

along curves of slope

$$\frac{dy}{dx} = \tan(\theta \pm m).$$

Values for $\omega = \omega(M)$ are given in column 3 of table 1.

(4) The shock-shock jump conditions for oblique shock-shocks are

$$\tan(\theta_1-\theta_0) = \frac{(M_1^2-M_0^2)^{\frac{1}{2}}(A_0^2-A_1^2)^{\frac{1}{2}}}{A_1M_1+A_0M_0}$$

and
$$\tan(\chi-\theta_0) = \frac{A_0}{M_0}\left(\frac{M_1^2-M_0^2}{A_0^2-A_1^2}\right)^{\frac{1}{2}},$$

Mach no. M	Ray area A $A \times 10^{-n}$	n	Characteristic angle m (degrees)	Prandtl–Meyer integral ω
1	∞		0	0
1·000001	3·668749	+10	—	0·003
1·00001	3·668672	+ 8	—	0·009
1·0001	3·667902	+ 6	0·403	0·028
1·001	3·660213	+ 4	1·280	0·089
1·01	3·584696	+ 2	4·002	0·283
1·05	1·310728	+ 1	8·544	0·633
1·10	2·946288	+ 0	11·474	0·896
1·15	1·184152	+ 0	13·142	1·097
1·20	6·053638	− 1	14·843	1·266
1·25	3·536658	− 1	15·958	1·414
1·30	2·250720	− 1	16·859	1·547
1·35	1·520662	− 1	17·604	1·669
1·40	1·074028	− 1	18·231	1·728
1·45	7·850741	− 2	18·766	1·887
1·50	5·898186	− 2	19·228	1·984
1·55	4·531934	− 2	19·630	2·077
1·60	3·548150	− 2	19·983	2·165
1·65	2·822580	− 2	20·295	2·249
1·70	2·276434	− 2	20·572	2·330
1·75	1·858064	− 2	20·820	2·406
1·80	1·532637	− 2	21·042	2·480
1·85	1·276079	− 2	21·242	2·551
1·90	1·071389	− 2	21·423	2·619
1·95	9·063299	− 3	21·587	2·685
2·00	7·719471	− 3	21·736	2·749
2·05	6·615861	− 3	21·872	2·811
2·10	5·702352	− 3	21·997	2·871
2·15	4·940726	− 3	22·111	2·929
2·20	4·301517	− 3	22·216	2·985
2·25	3·761766	− 3	22·312	3·040
2·30	3·303423	− 3	22·401	3·094
2·40	2·576553	− 3	22·560	3·203
2·50	2·037086	− 3	22·696	3·302
2·60	1·630023	− 3	22·814	3·388
2·70	1·318343	− 3	22·916	3·477
2·80	1·076566	− 3	23·006	3·563
2·90	8·868121	− 4	23·085	3·645
3·00	7·363072	− 4	23·154	3·724
3·20	5·184216	− 4	23·271	3·875
3·40	3·740925	− 4	23·364	4·015
3·60	2·757067	− 4	23·439	4·148
3·80	2·069662	− 4	23·501	4·272
4·00	1·578970	− 4	23·552	4·398
4·50	8·519558	− 5	23·647	4·660
5·00	4·926060	− 5	23·710	4·900
6·00	1·921342	− 5	23·788	5·314
7·00	8·705958	− 6	23·832	5·672
8·00	4·395269	− 6	23·859	5·966
9·00	2·408270	− 6	23·876	6·232
10·00	1·407051	− 6	23·889	6·470
15·00	1·786391	− 7	23·917	7·385
20·00	4·141420	− 8	23·926	8·033
100·00	1·172427	−11	23·937	11·67
∞	0		23·938	∞

TABLE 1

where index 0 refers to the flow before, index 1 to the flow behind, the shock-shock, θ_1 is the angle between the ray direction and the fixed co-ordinate system, and χ is the shock-shock angle between the shock-shock and the fixed co-ordinate system. The relationship between θ_1 and M_1 with M_0 as parameter ($\theta_0 = 0$) is shown in the form of hodograph shock-polars in figure 16; $(\chi - \theta_1)$ as a function of θ_1 with M_0 as parameter ($\theta_0 = 0$) is shown in figure 17.

Approximate analysis of shock-shock locus on cones of large semi-apex angle, $M_0 \gg 1$

For large semi-apex angles it can be assumed that the Mach shock is approximately straight (see figure 13). The velocity of point P is the same for both shocks, therefore

$$M_0 \sec \chi = M \sec (\chi - \theta). \tag{1}$$

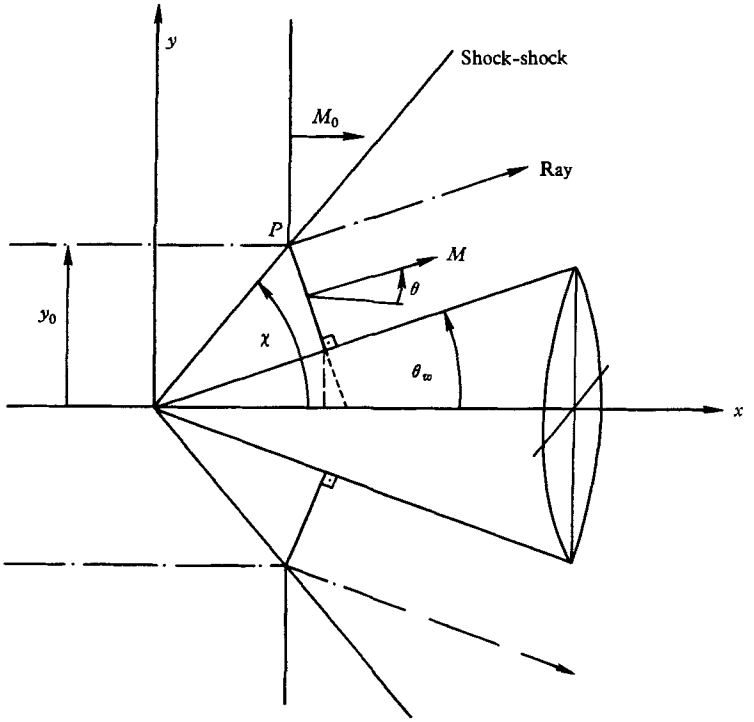

FIGURE 13

All the rays contained in the undisturbed ray tube of area $A_0 = \pi y_0^2$ must pass through a ray tube of area A behind the shock-shock, where

$$A = \pi y_0^2 \sec \theta \{1 - [1 - \cos \theta \csc \chi \sin (\chi - \theta)]^2\},$$

so that

$$\frac{A}{A_0} = \sec \theta \{1 - [1 - \cos \theta \csc \chi \sin(\chi - \theta)]^2\}. \tag{2}$$

But, for $M \gg 1$,

$$\frac{A}{A_0} = \left(\frac{M_0}{M}\right)^n \quad (n = 5{\cdot}0743), \tag{3}$$

assuming that this also holds across the shock-shock.

From (1), (2) and (3) we obtain a relationship between θ and χ, for $\theta \to \frac{1}{2}\pi$

$$\frac{\cos^n \chi}{\cos^n(\chi-\theta)} = 2\frac{\sin(\chi-\theta)}{\sin\chi} - \cos\theta\frac{\sin^2(\chi-\theta)}{\sin^2\chi}. \tag{4}$$

In the limit χ, $(\frac{1}{2}\pi-\theta) \ll 1$, (4) reduces to

$$\chi-\theta \simeq \tfrac{1}{2}(\tfrac{1}{2}\pi-\theta). \tag{5}$$

Equation (4) has been plotted in figure 12.

Approximate analysis of shock-shock locus on front of cylinders, $M_0 \gg 1$

It is again assumed that the Mach shock is almost straight and radial (see figure 14). Here the undisturbed rays contained in a stream tube of area $A_0 = (1+\lambda)\sin\phi$ pass through the area $A = \lambda$ per unit length of the cylinder.

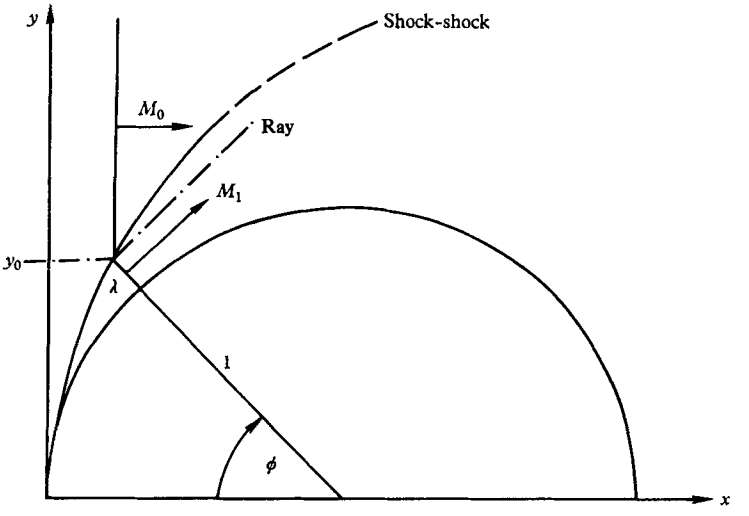

FIGURE 14

Mach shock and incident shock are parts of the same surface $\alpha(x, y, t)$ at any instant, where (Whitham 1959) in our case

$$\alpha = \alpha_0 t = \frac{x}{M_0} = \frac{1-(1+\lambda)\cos\phi}{M_0}. \tag{6}$$

By definition (Whitham 1959),

$$M|\nabla\alpha| = 1. \tag{7}$$

Since the Mach shock is normal to the wall, for the cylinder,

$$|\nabla\alpha| \simeq \frac{\partial\alpha}{R\,\partial\phi}. \tag{8}$$

Remembering that

$$\frac{A}{A_0} = \left(\frac{M_0}{M}\right)^n \quad (M_0 \gg 1),$$

we find a differential equation connecting λ and ϕ for $\phi \to 0$

$$\frac{d\lambda}{d\phi} = (1+\lambda)\tan\phi - \frac{1+\frac{1}{2}\lambda}{\cos\phi}\left[\frac{\lambda}{(1+\lambda)\sin\phi}\right]^{1/n}, \tag{9}$$

with the initial condition $\lambda = 0$ at $\phi = 0$ since at the nose the reflexion must be regular. In the limit $\lambda, \phi, (d\lambda/d\phi) \ll 1$ we find

$$\lambda = \sin^{n+1}\phi. \tag{10}$$

The solution of equation (9) is plotted in figure 15.

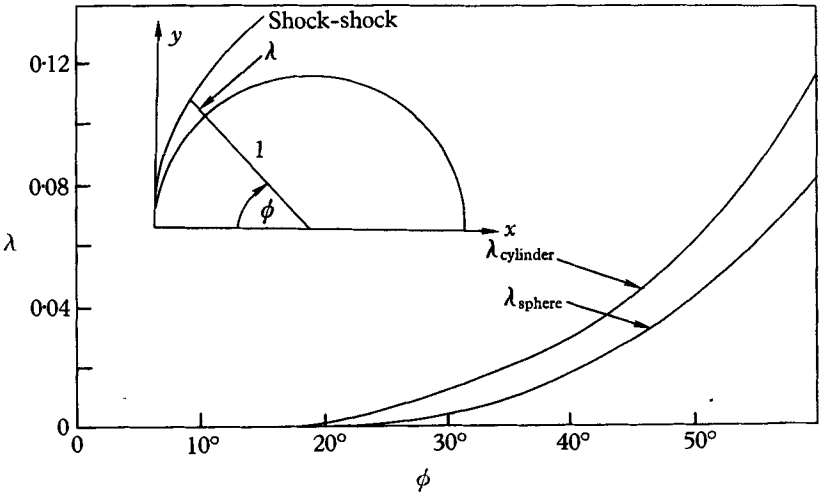

FIGURE 15. Position of shock-shock as given by approximate theory for blunt bodies, $M_0 \gg 1$.

Approximate analysis of shock-shock locus on front of sphere, $M_0 \gg 1$

The assumptions and notations are the same and equations (6), (7) and (8) hold also in this case, except that now

$$\left.\begin{aligned} A_0 &= \pi y_0^2 = \pi(1+\lambda)^2\sin^2\phi, \\ A &= 2\pi\lambda(1+\tfrac{1}{2}\lambda)\sin\phi. \end{aligned}\right\} \tag{11}$$

We obtain a differential equation analogous to (9), for $\phi \to 0$

$$\frac{d\lambda}{d\phi} = (1+\lambda)\tan\phi - \frac{1+\frac{1}{2}\lambda}{\cos\phi}\left[\frac{2(1+\frac{1}{2}\lambda)\lambda}{(1+\lambda)^2\sin\phi}\right]^{1/n}, \tag{12}$$

with $$\lambda = 0 \quad \text{at} \quad \phi = 0.$$

In the limit $\lambda, \phi, (d\lambda/d\phi)$ all $\ll 1$ the solution can be obtained explicitly

$$\lambda = \tfrac{1}{2}\sin^{n+1}\phi. \tag{13}$$

Very close to the nose the shock-shock 'stand off' distance on a sphere is half as large as on the cylinder for the same ϕ. The numerical solution obtained for (12) is also given in figure 15.

Assuming that the approximations for the positions of the shock-shock for cylinder and sphere are good up to $\phi = 50°$, we may chose a value of $\phi = 45°$, say, to find the shock-shock angle χ, shock-shock strength $(M_0/M_1)_s$, and ray angle θ_1

behind the shock-shock, which then can serve as a starting point for a characteristics solution (λ is so small near 45°, the shock-shock so close to the wall, that one point on the shock-shock appears sufficient).

The angle χ between the shock-shock and the x-axis is found, for the cylinder and the sphere, from

$$\tan\chi = \left(\frac{dy}{dx}\right)_{ss} = \frac{(1+\lambda)\tan\phi + d\lambda/d\phi}{(1+\lambda) - d\lambda/d\phi \,.\, \tan\phi}, \tag{14}$$

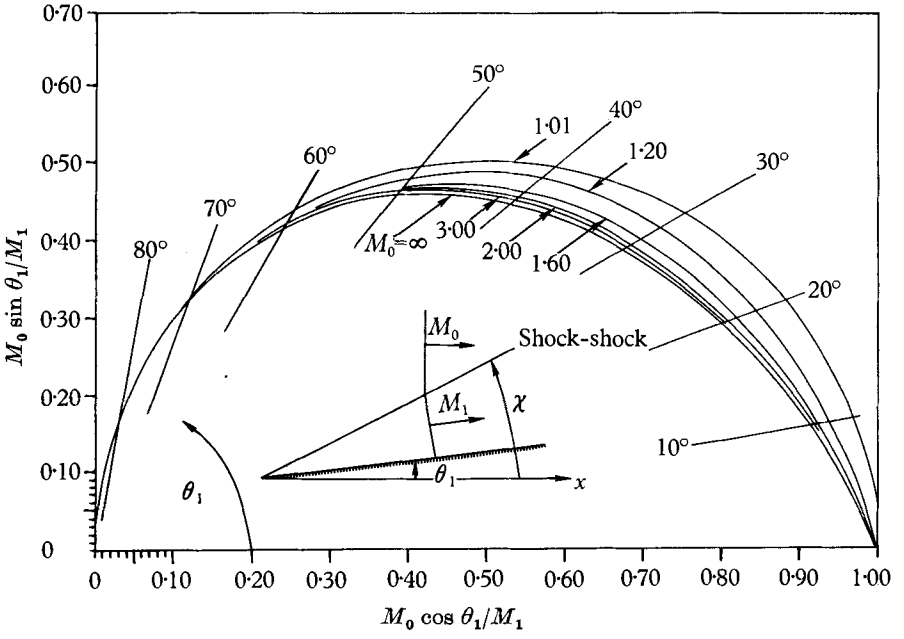

FIGURE 16. Shock-shock polars.

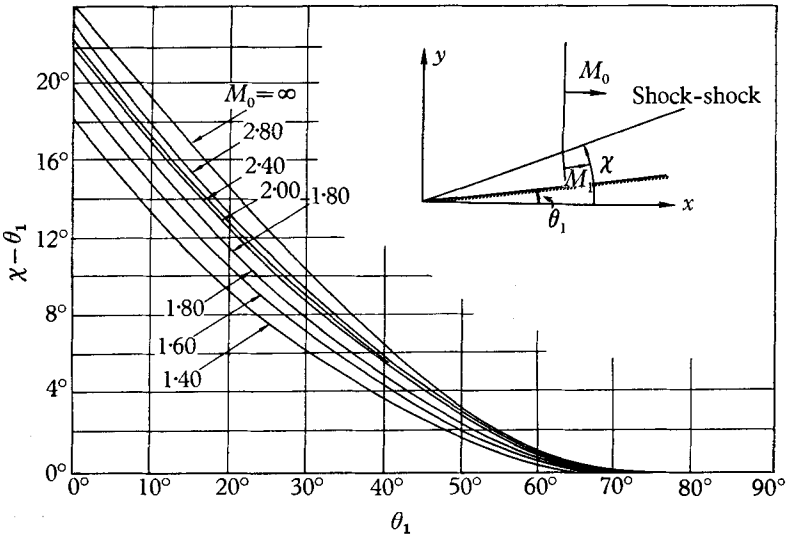

FIGURE 17. Shock-shock angle χ *vs* deflexion angle θ_1; shock-shock jump conditions; M_0 = incident Mach number.

where the origin of the x-y system is now located at the front stagnation point. Knowing χ, (M_0/M_1) and θ_1 are found from figures 16 and 17, and m from table 1. These values define the starting point for a characteristics solution in the physical and hodograph planes.

Characteristics solution for cylinder

If we neglect reflexions of the characteristics from the shock-shocks in this case, then the left-running characteristics are straight lines along which all flow properties are constant. In particular, the ray angle θ is constant between wall and shock-shock and equal to $\theta_{\text{wall}} = \frac{1}{2}\pi - \phi$. Knowing $\theta = \theta_w$, we may find (M_0/M_1) on the appropriate shock-shock-polar of figure 16, and the corresponding values for χ and m are given by figure 17 and table 1, respectively. This allows us to draw the left-running characteristic from any point on the wall. At the initial point 1 which lies on the shock-shock with χ, θ, M_0/M_1, and m given this scheme is inverted. The point 0 on the wall from which the left-running characteristic through the initial point issues is obviously defined by $\phi = \frac{1}{2}\pi - \theta$. From point 1 the shock-shock is continued with a slope $\tan\chi_3$, $\chi_3 = \chi(M_3)$, up to a point 3 where it intersects the characteristic from the next wall point 2. This semi-graphical method of constructing the shock-shock is illustrated by figure 18.

This procedure is continued up to $\phi = \frac{1}{2}\pi$; the characteristic from this point on the wall meets the shock-shock at infinity, $(M_0/M_1) = 1$ and $m = m_0$ along this characteristic.

The back side of the cylinder is obtained by a simple wave expansion along its wall. Again $\theta = \theta_{\text{wall}} = \frac{1}{2}\pi - \phi$ is known and assumed to be constant along a straight left-running characteristic. Then by means of the characteristic equation

$$\omega = -\theta,$$

where

$$\omega = \int_1^M \left[\frac{2}{(M^2-1)K(M)}\right]^{\frac{1}{2}} dM,$$

M and m are found from Table 1, $\omega = 0$ at $M = 1$ (which is in error in Whitham's paper of 1957).

When the diffraction reaches the plane of symmetry a second shock-shock is formed since the diffraction is again turned through a 'compressive' angle of $0 \leqslant \Delta\theta \leqslant \frac{1}{2}\pi$; the rays must be parallel to the plane of symmetry. All characteristics on the back side, therefore, intersect a second shock-shock. Observing that θ_1 (before the second shock-shock) is given and θ_2 (behind the second shock-shock) is equal to zero, χ can be found again from the shock-shock polar diagram, if we use the polar on which $M_0 = M_{\text{wall}}$. The second shock-shock starts at the rear stagnation point with $\chi = 0$, and is constructed piece-wise in the same manner as the first shock-shock.

Figure 6 shows the full characteristic field, the constructed shock-shapes and rays, and the experimental data. Also shown is the locus of the vortex in the slip surface, which should trace a particle path. The correspondence between theory and experiment appears to be good.

Characteristic solution for sphere

For axisymmetric shock diffraction problems, viz. a sphere, the characteristic equations in the hodograph plane have a term containing the radius r, which implies that the left-running characteristics are not straight lines. Also the diffraction around the back side is no longer a simple wave.

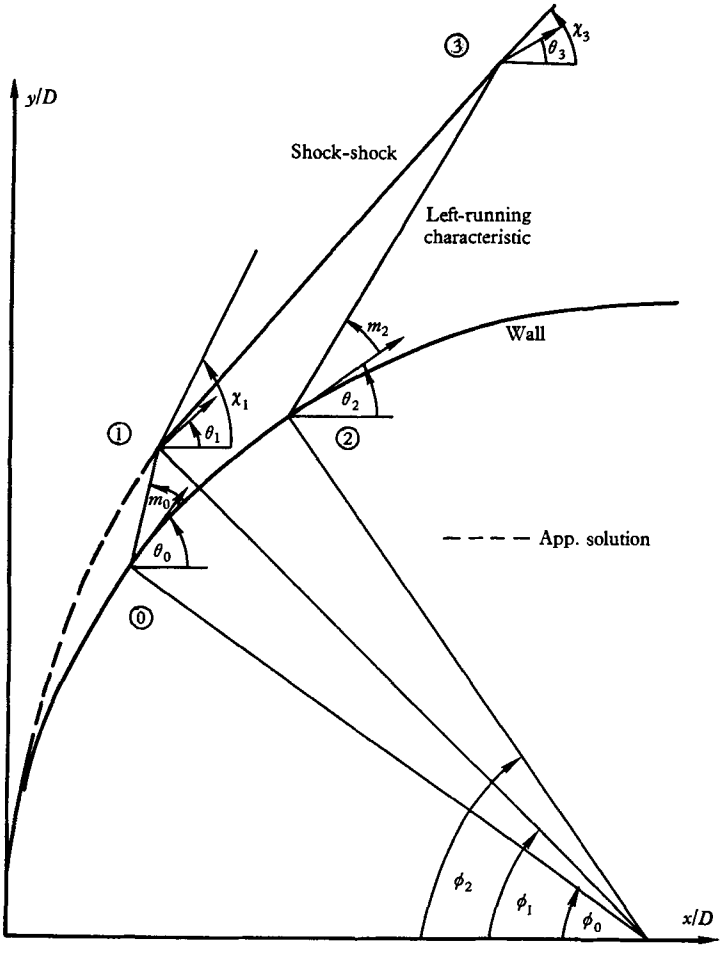

FIGURE 18

A purely graphical method proposed by de Haller (1945) and modified to apply to shock diffraction problems was used. Since the experimental incident Mach numbers were quite high, it was assumed that $M_0 \gg 1$. In this case the characteristic angle $m = 23{\cdot}9°$ becomes constant and independent of Mach number.

De Haller's method, also described in Shapiro (1954), solves the axisymmetrical characteristic equations in the physical and hodograph planes simultaneously making use of the two-dimensional hodograph characteristics, which are logarithmic spirals in our case. The term in the axisymmetrical characteristics equations containing the radius vector is found graphically in the physical plane and introduced as a correction term into the hodograph plane. A simple template

drawing device was made to mechanize the calculation. It was found, however, that the left-running characteristics in the hodograph plane became highly divergent on the aft portion of the sphere. A reliable solution for this part and the second shock-shock could, therefore, not be obtained.

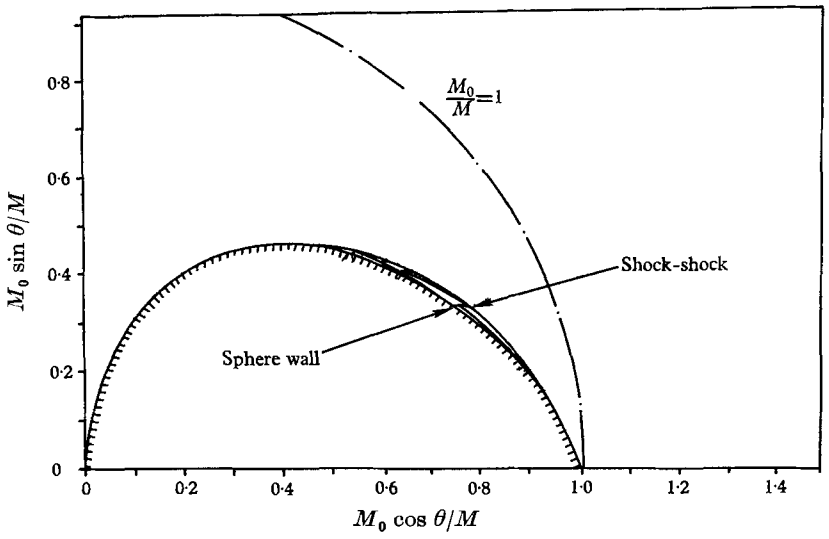

FIGURE 19. Hodograph plane for characteristics solution on a sphere fore-body, $M_0 \gg 1$. Numbers refer to successive points of the characteristic net in physical plane.

Figure 9 shows the result of the solution for the front of the sphere starting from an input point on the shock-shock as described previously. The experimental points for two different Mach numbers are also plotted. The correspondence appears to be very good. Figure 19 is a reproduction of the hodograph plane corresponding to this part of the diffraction field. It is seen that at an azimuth angle $\phi = 90°$, $\theta_{\text{wall}} = 0$ and the Mach number $(M_0/M_1) = 1$, as was found for the cylinder.

The experimental investigation was sponsored by the National Science Foundation under Grant 7008 to Harvard University, Cambridge, Mass. The theoretical calculations were sponsored by Douglas Aircraft Co. Inc., and performed on the Bendix G-15 computer at Douglas Aircraft Co. Inc., Missiles and Space Systems Engineering Department. We are particularly indebted to Mr W. A. Anderson, Douglas Aircraft Co. Inc., Santa Monica, for programming and performing the numerical calculations, and to Mr G. Brownell of Harvard University, Gordon McKay Laboratory machine shop for his unfailing assistance in the experiments.

REFERENCES

HALLER, P. DE 1945 *Revue tech. Sulzer*, no. 1.

SHAPIRO, A. 1954 *Dynamics and Thermodynamics of Compressible Fluid Flow*, vol. 2. New York: The Ronald Press.

WHITHAM, G. B. 1957 *J. Fluid Mech.* **2**, 145.

WHITHAM, G. B. 1958 *J. Fluid Mech.* **4**, 337.

WHITHAM, G. B. 1959 *J. Fluid Mech.* **5**, 369.

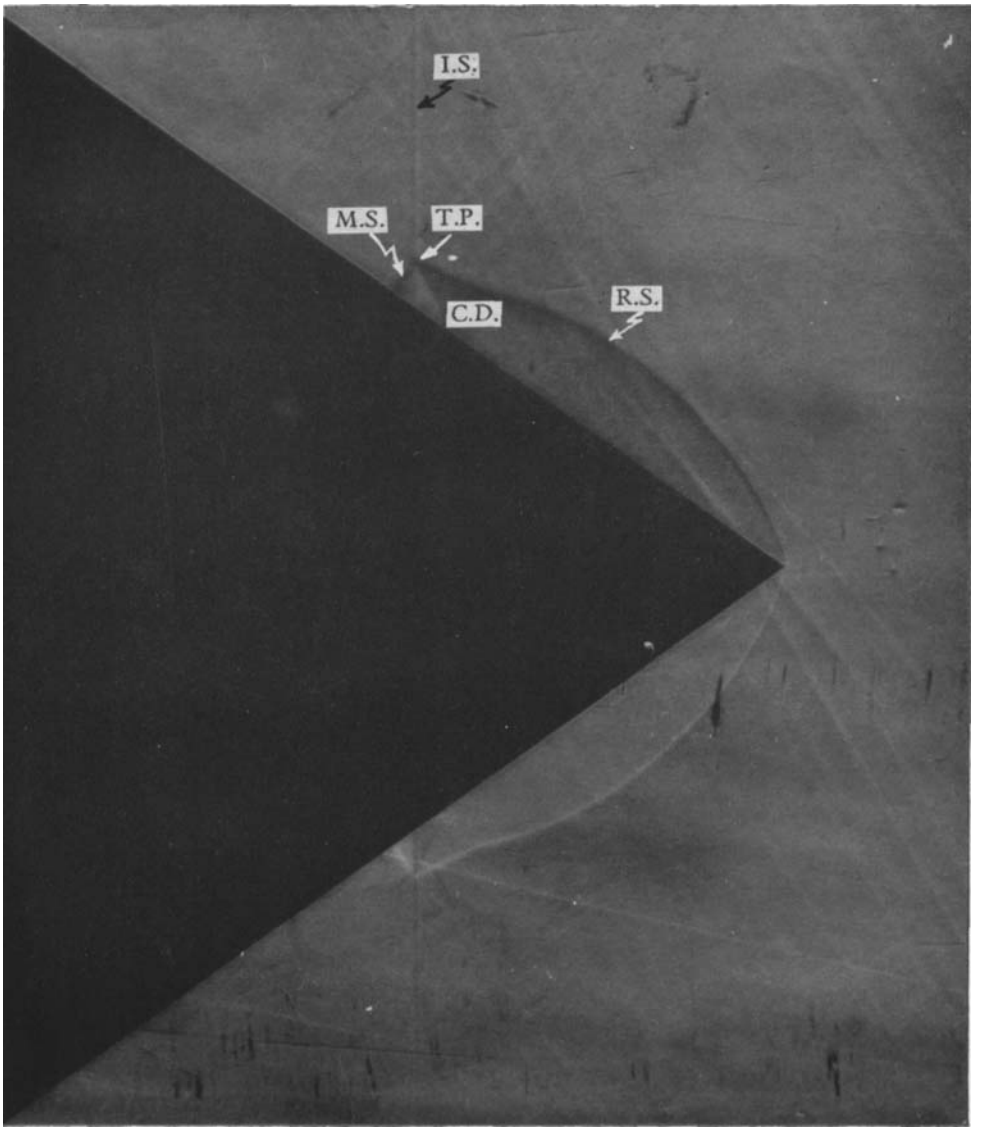

FIGURE 1 (plate 1). Schlieren photograph of shock diffraction on a cone of semi-apex angle $\theta_w = 35{\cdot}1°$. $M_0 = 3{\cdot}55$. Notation: I.S., incident shock; M.S., mach shock; R.S., reflected shock; C.D., contact discontinuity; T.P., triple point.

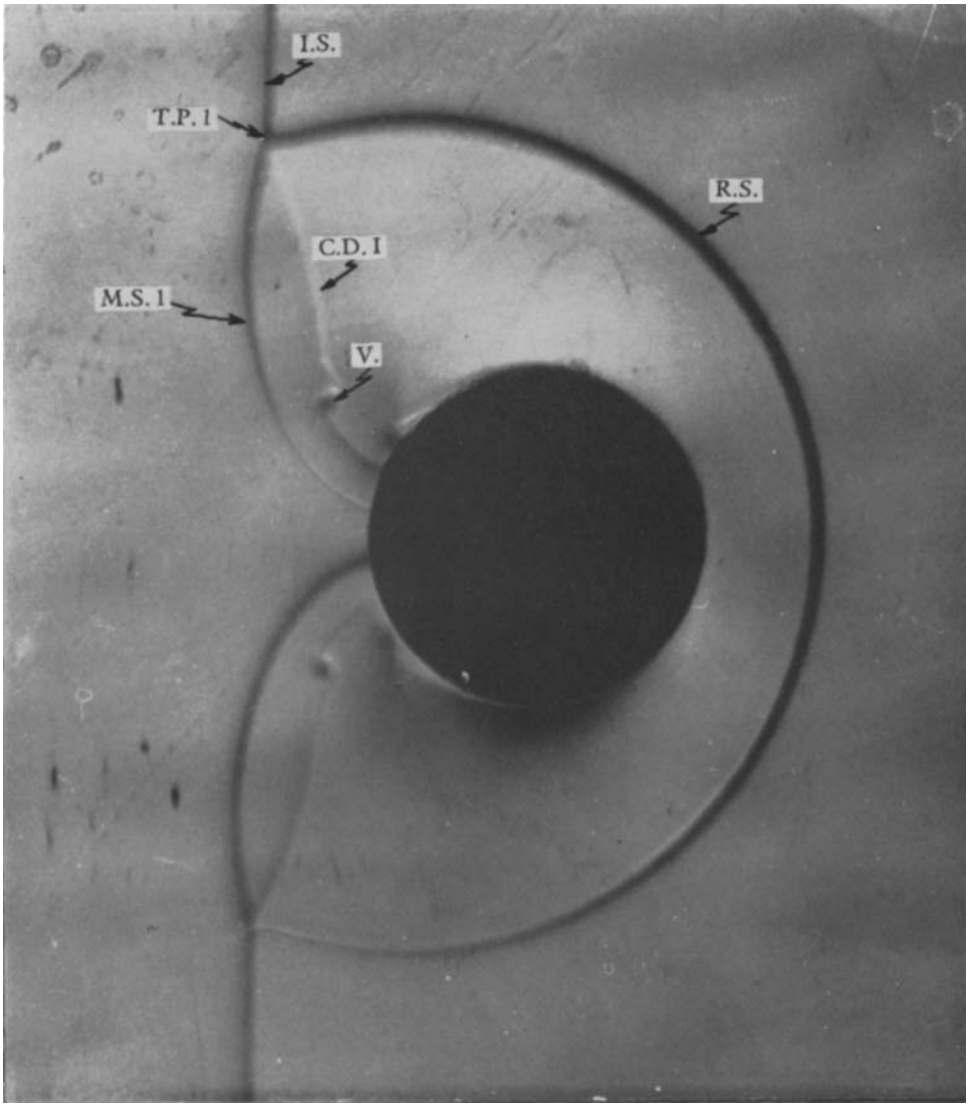

FIGURE 3 (plate 2). Schlieren photograph of shock diffraction on a cylinder of $\frac{1}{2}$ in. diameter. $M_0 = 2{\cdot}82$. Note the boundary-layer separation starting. Notation: I.S., incident shock; M.S., mach shock; R.S., reflected shock; C.D., contact discontinuity; T.P., triple point; V., vortex.

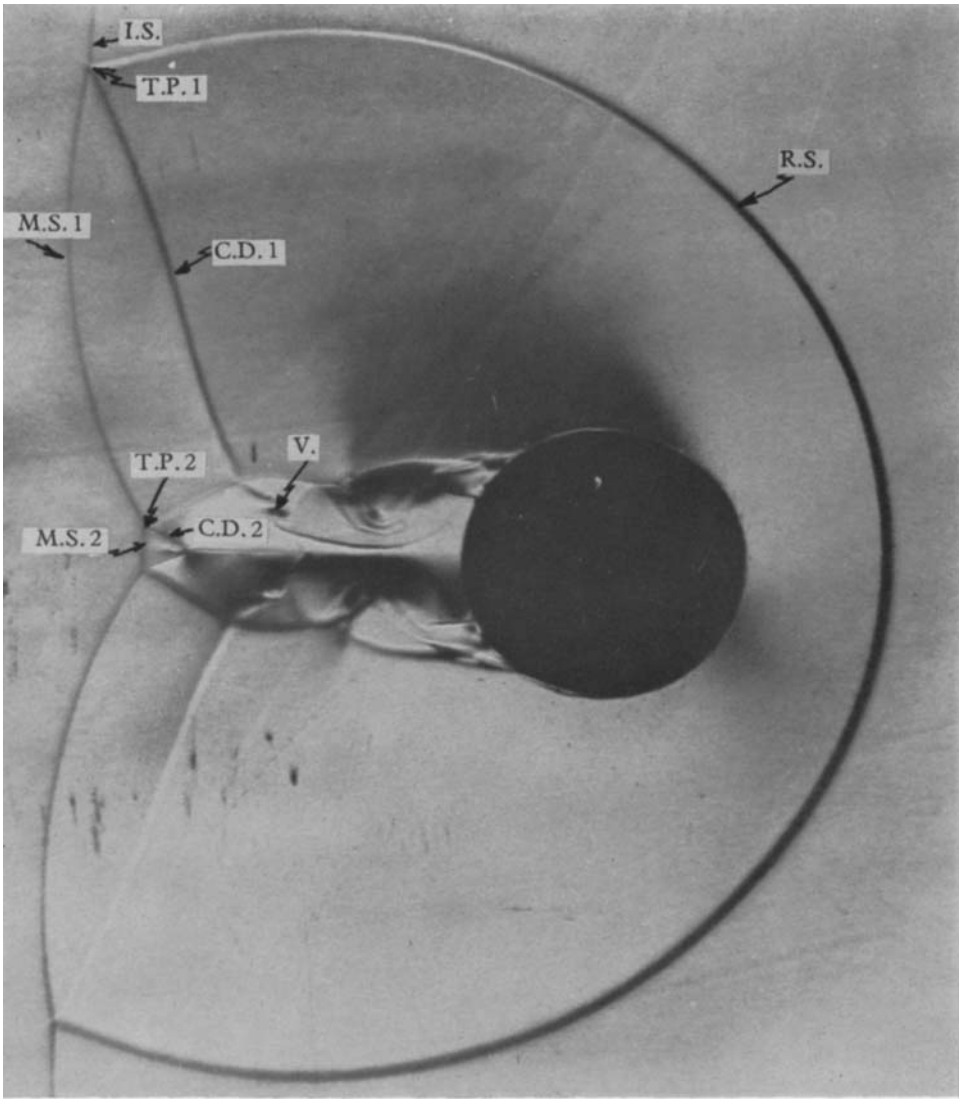

FIGURE 4 (plate 3). Schlieren photograph of shock diffraction on a cylinder of $\frac{1}{2}$ in. diameter. $M_0 = 2{\cdot}81$. Notation: I.S., incident shock; M.S., mach shock; R.S., reflected shock; C.D., contact discontinuity; T.P., triple point; V., vortex.

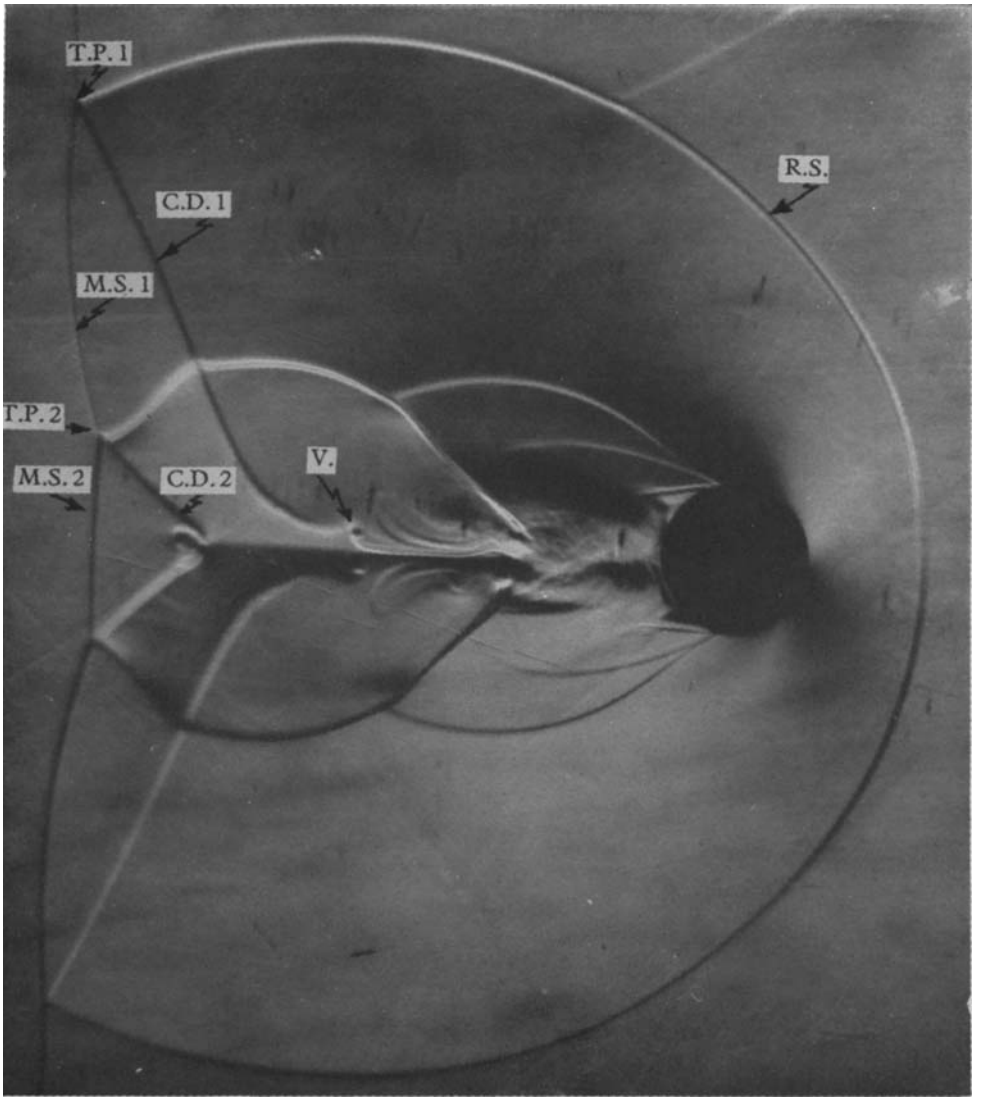

FIGURE 5 (plate 4). Schlieren photograph of shock diffraction on a cylinder of $\frac{1}{2}$ in. diameter. $M_0 = 2{\cdot}84$. Notation: M.S., mach shock; R.S., reflected shock; C.D., contact discontinuity; T.P., triple point; V., vortex.

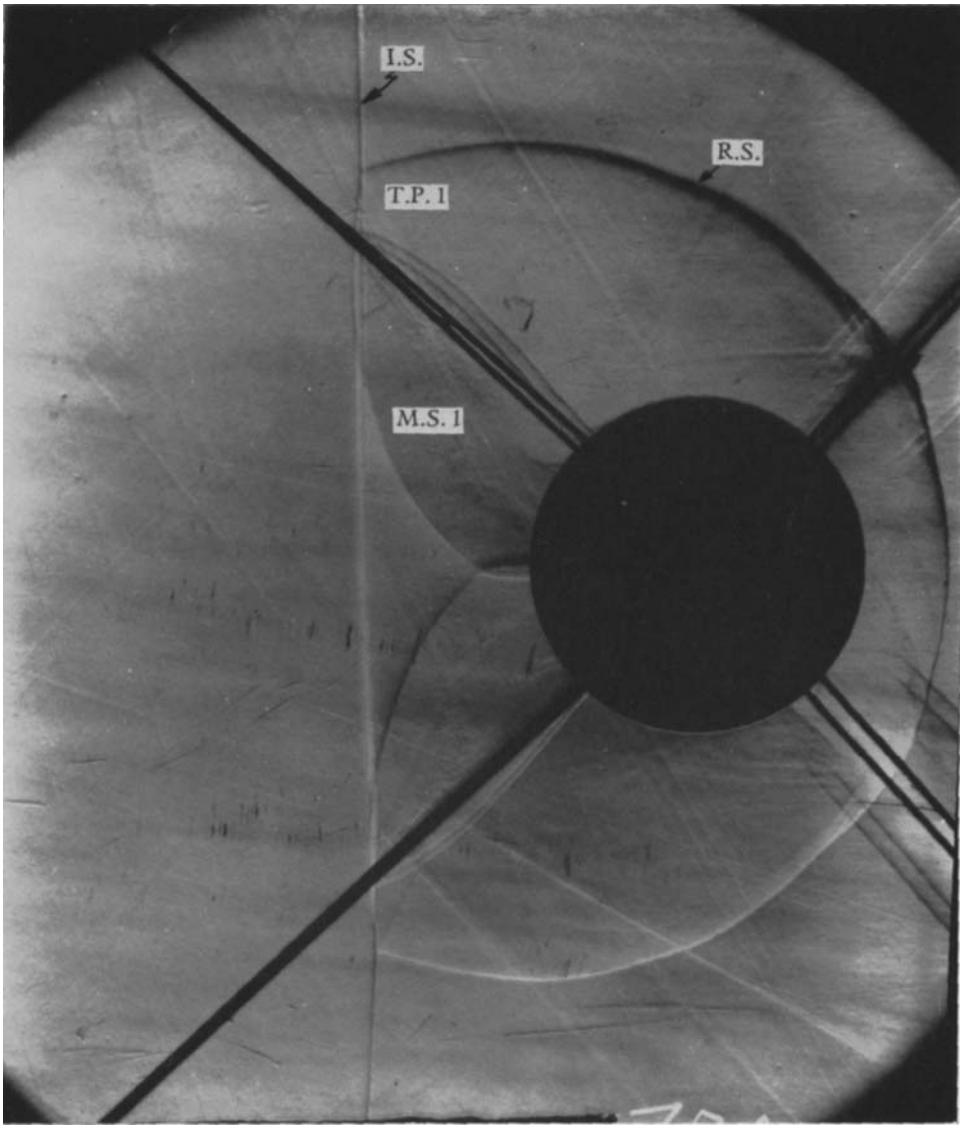

FIGURE 7 (plate 5). Schlieren photograph of shock diffraction on a sphere of 1 in. diameter. $M_0 = 2{\cdot}89$. Note the second Mach shock just forming. The eight radial lines are strings by which the sphere was suspended in the test section. Notation: I.S., incident shock; M.S., mach shock; R.S., reflected shock; T.P., triple point.

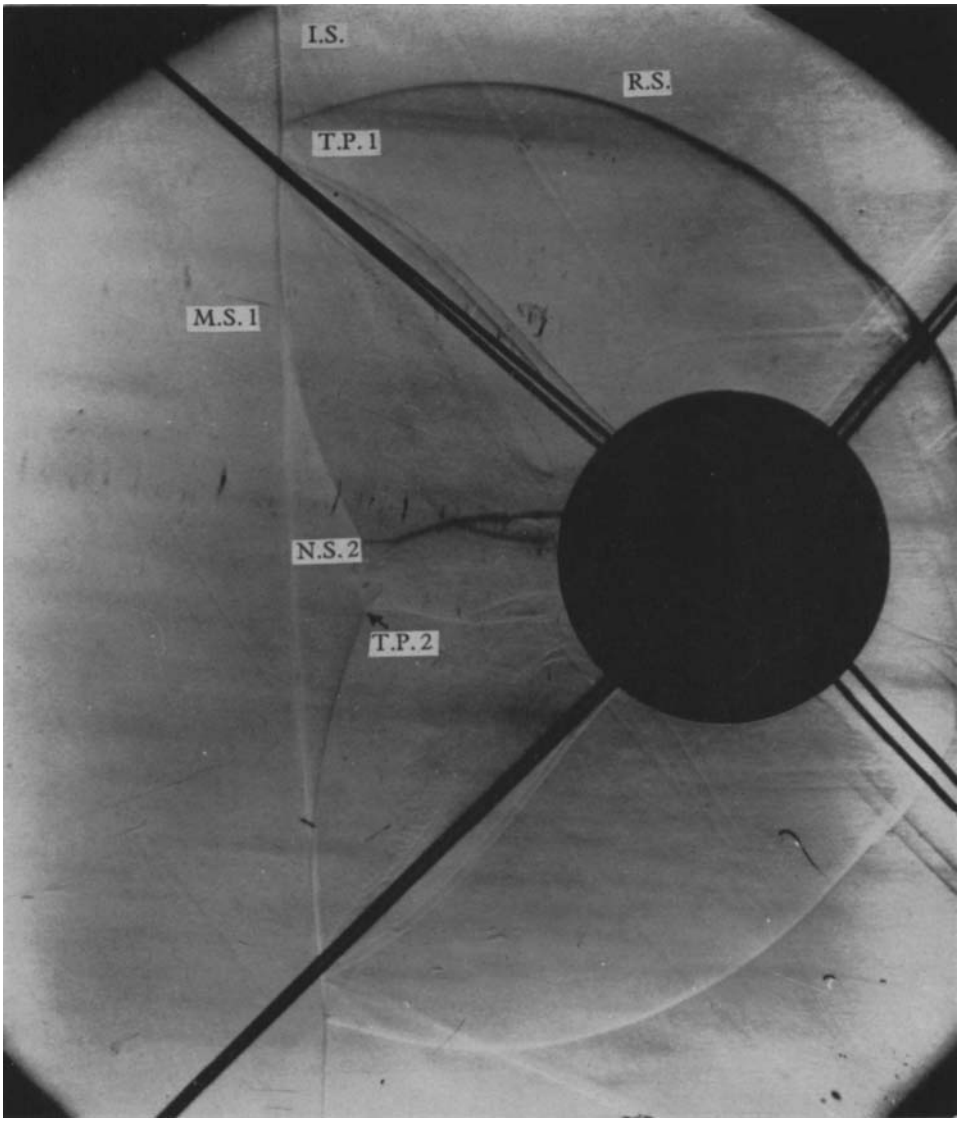

FIGURE 8 (plate 6). Schlieren photograph of shock diffraction on a sphere of 1 in. diameter. $M_0 = 2{\cdot}89$. Note the second Mach shock pierced by the spherical shock wave. Notation: I.S., incident shock; M.S., mach shock; R.S., reflected shock; T.P., triple point.